AGU PUBLICATIONS

JGR

Journal of Geophysical Research: Oceans

RESEARCH ARTICLE

10.1002/2017JC012984

Moored observations of the Deep Western Boundary Current in the NW Atlantic: 2004–2014

John M. Toole[1], Magdalena Andres[1], Isabela A. Le Bras[1], Terrence M. Joyce[1], and Michael S. McCartney[1]

[1]Woods Hole Oceanographic Institution, Woods Hole, Massachusetts, USA

Key Points:
- Moored observations spanning the NW Atlantic continental slope from 2004 to 2014 characterize the Deep Western Boundary Current
- The time-average intermediate and deep water equatorward transport is estimated to be 22.8 $\times$ 10^6 $\pm$ 1.9 $\times$ 10^6 m^3/s
- Statistically significant trends of reduced equatorward Deep Western Boundary Current transport with time are found over 2004–2014

Correspondence to:
J. M. Toole,
jtoole@whoi.edu

Citation:
Toole, J. M., M. Andres, I. A. Le Bras, T. M. Joyce, and M. S. McCartney (2017), Moored observations of the Deep Western Boundary Current in the NW Atlantic: 2004–2014, *J. Geophys. Res. Oceans*, *122*, 7488–7505, doi:10.1002/2017JC012984.

Received 11 APR 2017
Accepted 24 AUG 2017
Accepted article online 30 AUG 2017
Published online 15 SEP 2017

Abstract A moored array spanning the continental slope southeast of Cape Cod sampled the equatorward-flowing Deep Western Boundary Current (DWBC) for a 10 year period: May 2004 to May 2014. Daily profiles of subinertial velocity, temperature, salinity, and neutral density are constructed for each mooring site and cross-line DWBC transport time series are derived for specified water mass layers. Time-averaged transports based on daily estimates of the flow and density fields in Stream coordinates are contrasted with those derived from the Eulerian-mean flow field, modes of DWBC transport variability are investigated through compositing, and comparisons are made to transport estimates for other latitudes. Integrating the daily velocity estimates over the neutral density range of 27.8–28.125 kg/m^3 (encompassing Labrador Sea and Overflow Water layers), a mean equatorward DWBC transport of 22.8 $\times$ 10^6 $\pm$ 1.9 $\times$ 10^6 m^3/s is obtained. Notably, a statistically significant trend of decreasing equatorward transport is observed in several of the DWBC components as well as the current as a whole. The largest linear change (a 4% decrease per year) is seen in the layer of Labrador Sea Water that was renewed by deep convection in the early 1990s whose transport fell from 9.0 $\times$ 10^6 m^3/s at the beginning of the field program to 5.8 $\times$ 10^6 m^3/s at its end. The corresponding linear fit to the combined Labrador Sea and Overflow Water DWBC transport decreases from 26.4 $\times$ 10^6 to 19.1 $\times$ 10^6 m^3/s. In contrast, no long-term trend is observed in upper ocean Slope Water transport. These trends are discussed in the context of decadal observations of the North Atlantic circulation, and subpolar air-sea interaction/water mass transformation.

Plain Language Summary A sustained measurement program located southeast of Cape Cod observed the equatorward limb of the Atlantic Ocean overturning circulation for the period 2004–2014. The data are analyzed to document the time-averaged structure and volume transport of the Deep Western Boundary Current and explore its modes of variability. Integrating the daily velocity estimates over the Labrador Sea and Overflow Water layers, a mean equatorward DWBC transport of 22.8 $\times$ 10^6 $\pm$ 1.9 $\times$ 10^6 m^3/s is obtained. A statistically significant trend of decreasing equatorward transport is observed in several of the DWBC components as well as the current as a whole. These trends are discussed in the context of decadal observations of the North Atlantic circulation, and subpolar air-sea interaction/water mass transformation.

1. Introduction

In simplest terms, the Atlantic Meridional Overturning Circulation (AMOC) consists of a net northward transport of warm, buoyant waters in the upper ocean, and a compensating equatorward transport of colder, denser waters (usually at greater depth). Vorticity considerations place constraints on both limbs of the AMOC, as reviewed by *Stommel* [1957] and many others. For the deep water flow (in cases where the interior potential vorticity distribution is dominated by planetary beta), these dynamics suggest that the equatorward AMOC flow will be focused at the western boundary in a so-called Deep Western Boundary Current (DWBC). As an early element of the AMOC observing program (see https://usclivar.org/amoc), Line W was conceived to sample the DWBC about Lat. 39°N over an initial 10 year period using a combination of repeated ship observations, a moored array, and remote sensing products. Building on previous observations in the study region that extend back to the early days of the WHOI Buoy Group (http://www.whoi.edu/oceanus/feature/building-them-tough-bringing-them-back) and following 3 years of prototype/exploratory moored observations, the full Line W observing system was installed southeast of Cape Cod in May 2004 underlying a Topex-Poseiden altimeter satellite ground track, Figure 1. As discussed in earlier papers based

© 2017. American Geophysical Union. All Rights Reserved.

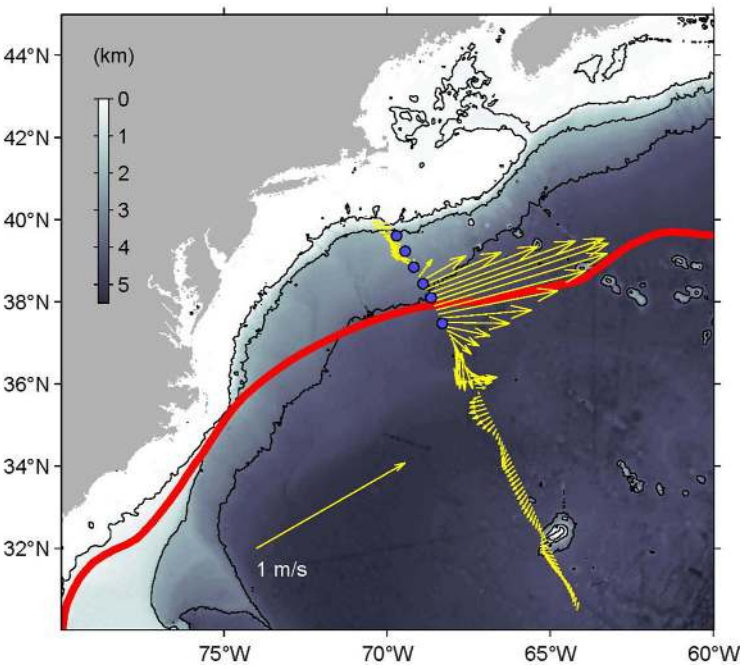

Figure 1. Map of the Northwest Atlantic Ocean bathymetry (shading with color bar over land) showing the location of the Line W moorings (blue dots) and time-average axis of the Gulf Stream (red line—taken as a specified mean sea surface height contour). The yellow arrows depict the mean surface geostrophic velocity on Line W in the 2004–2014 period for the subset of times when the Gulf Stream and its North Wall were near their mean crossing latitudes at the Line and there were no strong surface velocity anomalies in the Slope Water. The 200, 2000, and 4000 m isobaths are highlighted. The surface geostrophic velocity and Gulf Stream axis location are based on altimetric-derived sea surface height estimates (see text).

on those previous observations and measurements from the first 4 years of Line W [e.g., *Joyce et al.*, 2005; *Toole et al.*, 2011; *Peña-Molino et al.*, 2011, 2012], the equatorward DWBC flow at Line W is confined between the poleward-directed Gulf Stream and the continental slope. So rather than the canonical vertical partitioning of the AMOC typical of latitudes south of the Gulf Stream separation latitude around Cape Hatteras, at Line W the cold and warm limbs of the principal AMOC flows appear essentially side-by-side. Thus, partitioning of the AMOC branches at these more northerly latitudes must be guided by the direction of meridional flow at each water density horizon rather than a simple subdivision by depth of the horizontally averaged velocity.

Using similar methodologies, the present work extends the *Toole et al.* [2011] analysis of data from the period May 2004 to April 2008 to characterize the DWBC velocity and transport over the full 10 years of the now-completed Line W field program. Section 2 that follows (and Appendix A) presents the observations and data products we analyze. The 10 year Eulerian-mean fields are discussed in section 3, followed by analysis of the DWBC transport (section 4), and an examination of DWBC variability modes that involves compositing exercises (section 5). Comparisons of the Line W DWBC mean transport to estimates at other latitudes are made in section 6. The paper concludes with a general discussion of the results. Companion papers by *Smith et al.* [2016], *Andres et al.* [2016, 2017], and *Le Bras et al.* [2017] discuss the water property observations at Line W in the context of eddy variability, exchange with the ocean interior, and regional decadal change in the Northwest Atlantic Ocean.

2. Data and Products

Subsurface moored observations were obtained from six sites (identified as W1–W6, shallow to deep) spanning the continental slope southeast of Cape Cod between depths of 2238 and 4700 m (Figure 1 and Table A1). The data product that forms the basis of the present analysis consists of daily realizations of the subinertial temperature, salinity, and velocity profiles at each mooring site over the period 11 May 2004 to 27 April 2014. The subsurface moorings were a mix of conventional installations having discrete sensors distributed vertically along the wire and Moored Profiler moorings that supported both discrete and profiling instrumentation. The configuration of the array changed over time; details are provided in Appendix A. Most notably, the offshore most mooring (W6) was effectively on station for only the 2008–2014 period. In addition, W4 for the 2011–2012 period was lost in its entirety, the full recovery and redeployment of the moored array in 2008 was delayed due to bad weather on multiple cruises (causing extended data gaps when instruments exhausted their batteries before recovery) and some individual sensors suffered catastrophic failure. Despite such difficulties, overall data return from the mooring program was good with information being returned from multiple depths from virtually every mooring setting. Various methods of interpolation and extrapolation were carried out to obtain the homogenous data set analyzed here (see

Table 1. Layer Definitions and Bounding Neutral Density Surfaces for Transport Calculations[a]

Layer Name	Neutral Density (kg/m^3)	Average Depth (m)
	0.0	0
SURF	27.800	754.4
ULSW	27.897	1158.7
CLSW	27.983	1990.1
ISOW	28.066	2788.1
DSOW	28.125	3645.2

[a]Key: SURF, Upper Ocean Slope Water; ULSW, Upper Labrador Sea Water; CLSW, Classical Labrador Sea Water; ISOW, Iceland-Scotland Overflow Water; DSOW, Denmark-Strait Overflow Water. Average depths are based on means across moorings W1–W5.

Appendix A). Regardless of mooring type, sensor data were low-pass filtered to remove near-inertial and super-inertial period signals (either by digital filtering of time series data or by averaging bursts of profiles) and bin-averaged or interpolated onto a uniform 2 dbar grid. In this analysis, velocity data are rotated 60° clockwise to an across-line and along-line coordinate system; flow across the measurement line will be termed poleward or equatorward.

The Line W moored measurements were augmented with surface geostrophic velocity estimates based on the absolute dynamic topography produced by Ssalto/Duacs and distributed by AVISO, with support from CNES (http://www. aviso.altimetry.fr/duacs/). Both the data along the Jason-2 (and previously Jason-1 and Topex/Poseidon) satellite track number 126, and the 1/4°—resolution surface geostrophic velocity product based on data from multiple satellites were used. The former provides information at high-spatial resolution albeit along one line (allowing one component of the surface geostrophic velocity to be estimated) at 10 day temporal resolution while the latter product uses data from multiple satellites and a mapping procedure to derive both components of the horizontal flow at 1 day interval.

The chief foci of the Line W program are the intermediate and deep water masses. Consequently, the moored measurements concentrated on waters below 500 m. For completeness here, full-depth profiles were derived by extrapolation and interpolation. The daily subinertial velocity profiles from the moored instruments were linearly interpolated between the top current sensor on each mooring and the sea surface using the daily gridded AVISO surface geostrophic velocity estimates based on altimeter observations. Temperature and salinity profiles from the moored instruments were extrapolated above their shallowest measurement level using available ship station observations, adjacent mooring observations, and vertical heave assumptions (see Appendix A). Spatial integrations of the across-line velocity component yielded estimates of DWBC meridional transport. Building on *Toole et al*. [2011], DWBC transport estimates are reported for layers bounded in the vertical by specified neutral density values, Table 1, and in the horizontal by the continental slope and various offshore limits (described in section 4). For consistency with that earlier work, the layer names are retained here, but it is recognized that Labrador Sea Water properties vary annually [*Yashayaev and Loder*, 2016] and there is no one set of layer definitions that may be judged as the ideal. The layer termed here as Classical Labrador Sea Water corresponds most closely to the cold, dense waters produced by intense winter convection in the early 1990s. Upper Labrador Sea Water encompasses lighter modes of intermediate water that are found subsurface at Line W. Similarly, the exact definitions and nomenclature of the denser DWBC layers vary between researchers and study regions. In section 6, we compare Line W transport estimates with selected published values for other regions using common layer definitions.

3. Eulerian Time-Mean Fields

A Line W Eulerian-mean velocity section was derived from the available daily profile estimates by averaging on pressure surfaces, Figure 2. (Averaging velocity on density surfaces and mapping to the mean depths of isopycnals gave very similar results, so the simpler approach is adopted here.) Similar to the image constructed from the first 4 years of data [see *Toole et al*., 2011, Figure 3], in the 10 year mean, equatorward DWBC flow is located in a wedge between the continental slope and the inclined North Wall of the Gulf Stream. The mean along-line component of flow is weakly on-shore shallower than W4 (near the boundary between the mean DWBC and Gulf Stream) and is offshore at the deeper mooring sites (Figure 2b). Both suggest that Line W (oriented to underlie a satellite ground track) is not perfectly orthogonal to the mean flow. The mean flow is more zonal—and more aligned with the local isobaths—than the direction orthogonal to the satellite track. The poleward Gulf Stream jet is broadened and weakened in this mean picture relative to synoptic realizations due to meandering. Warm Core Gulf Stream Rings [e.g., *Joyce*, 1984; *Joyce and*

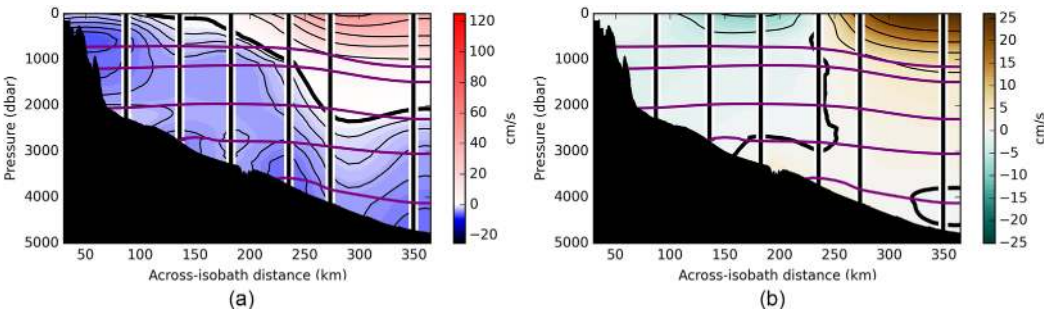

Figure 2. Contour plot of the Line W Eulerian-mean (a) across-line and (b) along-line velocity based on the 2004–2014 Line W moored observations and surface geostrophic velocity estimates derived from altimeter data. The average profiles at moorings 1–5 are based on the full 10 year record of observations; that at mooring 6 derives from data obtained between 2008 and 2014 only. The mean depths of the neutral density surfaces chosen to partition the water column and location of the moorings are also indicated. In Figure 2a, the contour interval for the across-line component is 1 cm/s for equatorward-directed currents and 10 cm/s for poleward. The zero isotachs are marked with thick black lines. The contour interval for Figure 2b is 5 cm/s.

Kennelly, 1985] and deep cyclones related to offshore Gulf Stream meanders [*Savidge and Bane*, 1999a,1999b; *Andres et al*., 2016, 2017] also greatly influence this Eulerian mean (see below).

Weak but statistically significant cores of enhanced equatorward flow at the bottom are evident in the 10 year Eulerian mean at moorings W2, W4, and W6. (Recall that the W6 record does not span the full 10 years.) In addition, a marginally significant middepth equatorward velocity extremum is seen at W1. These features are reminiscent of the composite analysis of deep currents in the Mid-Atlantic Bight reported by *Watts* [1991]. That compilation of moored current meter data principally from the 1974 to 1986 period along and west of 70°W suggested coherent bands of enhanced equatorward near-bottom flow at 3400–4500 m and $\theta \leq 2$°C, around 2500 m and 2.9°C $\leq \theta \leq$ 3.0°C and between 800 and 1100 m with 4.0°C $\leq \theta \leq$ 4.3°C. The Line W 10 year-mean velocity cores are at 3700 dbar/1.9°C (W4), 2700 dbar/2.5°C (W2), and 550–700 dbar/ 5.0°C $\leq \theta \leq$ 5.75°C (W1). The mean potential temperature at the bottom of W6 (4700 dbar) is 1.8°C. While the mean velocity core speeds observed on Line W (5–6 cm/s) are in the range of those reported by Watts, the correspondence in potential temperature is not particularly compelling. Moreover, the eddy mechanisms responsible for the Line W velocity cores at W1 and W6 (see the following and section 5) argue against these latter features being contiguous flows within the Mid-Atlantic Bight.

The most striking difference between this 10 year mean across-line velocity field and that based on the 2004–2008 period presented by *Toole et al*. [2011] is the deep equatorward mean flow at the seaward end of the array (an admittedly misleading comparison given that W6 was not on station for most of that earlier period and what data were available from that time were not used when constructing that earlier mean section). The 2004–2008 data suggested that the mean abyssal equatorward flow was confined between the shelf break and W5 whereas the Eulerian-mean velocity at W6 for the 2008–2014 period exhibits a marked equatorward flow at the bottom. As is argued later, this W6 mean velocity feature appears to be the product of deep cyclonic eddy features associated with southward meanders of the Gulf Stream [*Andres et al*., 2016, 2017]. For comparison, a "reference" or "ideal" Eulerian-mean section was constructed based on the moored observations from those days when the Gulf Stream core and North Wall were close to their mean locations along Line W

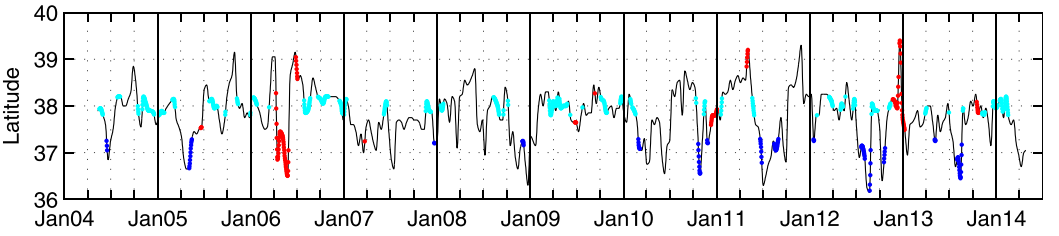

Figure 3. Time series of the Gulf Stream's velocity core latitude where it crosses Line W (black line) based on satellite altimeter data. Core latitude on days selected for the ideal state composite section are marked with cyan dots while the blue dots indicate days when there were large Gulf Stream southward meanders at Line W but no strong Slope Water surface velocity anomalies. Red dots mark times when the surface velocity at mooring W1 were strongly poleward (interpreted as times when a Warm Core Ring lay on Line W).

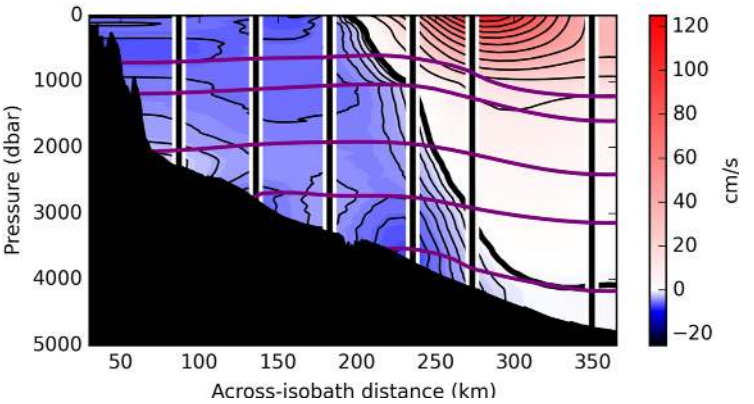

Figure 4. Composite Line W across-line velocity section constructed from observations on days when the Gulf Stream velocity core and North Wall were near their time-averaged locations and no strong surface velocity anomalies were present in the Slope Water. Contour interval is 1 cm/s for equatorward flows and 10 cm/s for poleward velocities; the thick black line marks the zero isotach.

and there were no anomalously strong surface velocities between the North Wall and shelf break. To identify this data subset, the altimeter-based across-line surface geostrophic velocity estimates were examined to identify the time-varying latitude of the velocity core of the Stream, the latitude of the first velocity zero crossing of the cross-line flow north of the velocity core (identified as the North Wall position), and the strongest positive and negative across-line velocities in the Slope Water north of the North Wall. In general, good agreement was found between the altimeter-based latitude of the Gulf Stream axis and the more traditional definition based on subsurface temperature—e.g., location where the temperature at 200 m depth equals 15°C [*Fuglister and Voorhis*, 1965] for the times when the latter was positioned within the lateral extent of the moored array. The altimeter metrics were adopted as they were available consistently throughout the field program. These 10 day estimates were interpolated to daily values to match the moored records, and then the times when the Gulf Stream core fell between 37.8°N and 38.2°N (Figure 3), the North Wall was between 38.5°N and 38.9°N, the Slope Water poleward surface velocity was everywhere less than 10 cm/s and the equatorward Slope Water surface velocities were less than 30 cm/s were identified and this subset of profiles from each mooring were averaged. The resulting composite velocity section, Figure 4 (the average surface velocities for this subset are also displayed in Figure 1), represents 16% of the available daily profiles in the 10 year record. So while this composite might be considered an image of the ideal state of the DWBC and Gulf Stream at Line W, the ocean was rarely in that exact configuration.

Comparing Figures 2 and 4, several differences are evident. First, the Gulf Stream jet is much stronger and narrower in the ideal composite since the selection criteria excluded times when the Stream had meandered away from its average latitude on Line W. Second, whereas the full Eulerian mean at W1 has a subsurface equatorward extremum around 500 m depth (marginally significant at the 95% confidence level), the ideal composite equatorward velocity at this site increases monotonically with height nearly to the surface. It is argued below that the W1 subsurface extremum in the 10 year mean is a consequence of Gulf Stream Warm Core Rings. And third, at W6 the ideal composite has near-zero meridional flow at depth, in contrast to the 10 year mean. (The mean bottom velocity at W6 in the ideal composite of −0.5 cm/s is not statistically different from zero at 95% confidence.) A contrasting composite analysis presented below that focuses on times when the Gulf Stream was displaced south documents the strength of the deep cyclones that are present at times of southward meanders and their influence on the 10 year Eulerian mean. Interestingly, the two equatorward velocity cores at the bottom of moorings W2 and W4 seen in the 10 year mean are also evident in the ideal composite that includes far less data than the original series.

4. Volume Transport

DWBC meridional transport at Line W was estimated for layers bounded in the vertical by neutral density surfaces, Table 1. Transport estimates were derived for each daily realization of the velocity/density fields as well as for the time-averaged fields. For a given velocity and density field, a running horizontal integration (using the rectangle method starting at the continental slope) of the vertically integrated, across-line velocity between specified neutral density bounds was performed, yielding the layer transport stream function versus offshore distance. For each layer and realization of the velocity and density field, the most equatorward (negative) value of the stream function within the horizontal span of the moored array was taken as

Table 2. Mean Equatorward DWBC Transport and 10 Year Linear Trend Estimates Partitioned by Water Mass Layer[a]

Layer	Eulerian 10 Year Average	Eulerian Ideal-Case Composite	Average of Daily Transports With Uncertainty	Integral Time Scale	Line W 10 Year Trends With Uncertainty	ECCO 40°N Mean Net Transports With Uncertainty	RAPID 26.5°N Mean Net Transports
SURF	−2.45	−6.62	−6.83 ± 0.42	12.2	0.004 ± 0.10	13.28 ± 1.36	16.73
ULSW	−2.66	−3.74	−4.33 ± 0.46	13.2	0.08 ± 0.04	−1.47 ± 0.12	−0.92
CLSW	−5.06	−6.20	−7.37 ± 1.20	14.7	0.32 ± 0.06	−5.67 ± 0.51	−5.66
ISOW	−3.97 (–4.97)	−4.39	−5.77 ± 0.93	8.9	0.24 ± 0.06	−5.58 ± 0.41	−4.77
DSOW	−3.74 (–6.14)	−3.31	−5.29 ± 0.50	4.7	0.09 ± 0.06	−1.10 ± 0.44	−2.56
Four-layer sum	−15.43 (–18.83)	−17.64	−22.76 ± 1.38	10.5	0.74 ± 0.20	−13.83 ± 1.00	−13.91
Five-layer sum	−17.88 (–21.28)	−24.26	−29.59 ± 2.08	11.9	0.74 ± 0.25	0.55 ± 0.37	2.82

[a]Reported mean transports (negative values denoting equatorward transport in units of 10^6 m^3/s) represent the most equatorward values of the across-line transport stream functions evaluated over moorings W1–W5. Values given within parentheses consider the transport stream functions extended to mooring W6 if different from those truncated at W5. Shown are the estimates for the full 10 year Eulerian-mean fields (W6 only for the 2008–2014 period), the ideal-case Eulerian mean, and the means of the daily DWBC transport estimates in Stream coordinates. Statistical uncertainties reported for the latter represent 95% confidence bounds based on degrees of freedom derived from integral time scales (also reported in days). The four-layer sum encompasses the two Labrador Sea and two Overflow Water masses while the five-layer sum adds the surface layer. Linear trend estimates of the daily Line W DWBC transports for each layer ($\times 10^6$ $m^3/s/yr$, again evaluated over moorings W1–W5) are given with 95% statistical uncertainties based on a bootstrap procedure. The ECCO and RAPID columns present estimates of the time-mean net meridional layer transports (ECCO for the Line W measurement period, RAPID for the interval April 2004 to October 2015). For ECCO, 95% uncertainty estimates are given based on (a conservative) 10 degrees of freedom. Annual-mean AMOC strength estimated from the RAPID observations is said to have an uncertainty of around 1×10^6 m^3/s (Smeed, personal communication, 2017). Assuming successive annual-mean values are independent yields layer transport uncertainty comparable to those of the ECCO results.

the layer's transport estimate. In general, the horizontal integrations to derive the stream functions were extended as far as W5; in certain cases the calculations were run to W6.

The transport estimates based on the 10 year Eulerian-mean velocity and density fields integrated to W5, Table 2, are marginally smaller than those reported by *Toole et al*. [2011, their Table 4] based on the first 4 years of data. Extending the stream function integrations of the 10 year Eulerian-mean flow field to W6 adds 3.4×10^6 m^3/s of equatorward DWBC flow coming from the Overflow Water layers. Transports integrated over the full width of the array without considering the location of the stream function minimum have smaller magnitude in the shallower layers owing to the poleward influence of the Gulf Stream flow on the offshore side of the array (values not shown). Equatorward mean transports derived from the ideal composite velocity field (calculated in identical fashion) are greater than those for the full 10 year Eulerian-mean velocity field in the intermediate water layers and less in the overflow layers, as might be expected comparing Figures 2 and 4.

For consistency throughout the 10 year observing period (and to facilitate comparison to the prior analysis of the 2004–2008 observations), daily layer transports were obtained as described above using layer transport stream functions that were integrated from the continental slope to mooring W5. As is quite evident in Figure 5, the variability of the intermediate and deep water layer transports across Line W is huge, with the four-layer summed transports ranging in time from (nearly) zero to more than 70×10^6 m^3/s. No obvious periodicity is evident in the transport time series. Energy-density spectra of the layer transport time series are relatively flat for periods between annual and ~90 days and follow a −2 frequency power law at shorter periods to a noise floor around 3 day period. Least square fits to the annual harmonic in each layer returned amplitudes ranging between 0.1 and 0.4×10^6 m^3/s (explaining less than 1% of the respective transport variance in each layer) with time of maximum transport varying between late March and mid-June. Integral time scales (derived by integrating the autocorrelation functions from the zero-lag point to their first zero crossings) fall from 13 to 15 days for the Labrador Sea Water layers to 5–9 days for the overflow layers, possibly due to bottom-enhanced Topographic Rossby Waves known to have energy at 10 day period and longer around Line W [*Thompson*, 1971; *Fratantoni and Pickart*, 2003; *Peña-Molino et al*., 2012]. We note however, that TRW signals may be minimized by the present transport estimation scheme that integrates horizontally to stream function extrema (and thus tends to integrate to the same phase of a spatially oscillatory velocity pattern superimposed on a larger-scale current).

We find that the largest fraction of the Line W transport variance is attributable to changes in layer-averaged velocity. DWBC layer transport may be expressed as the triple product of layer-width (W), layer-thickness (H) and layer-averaged velocity (V), each of which comprised of a time-average value plus fluctuations about the

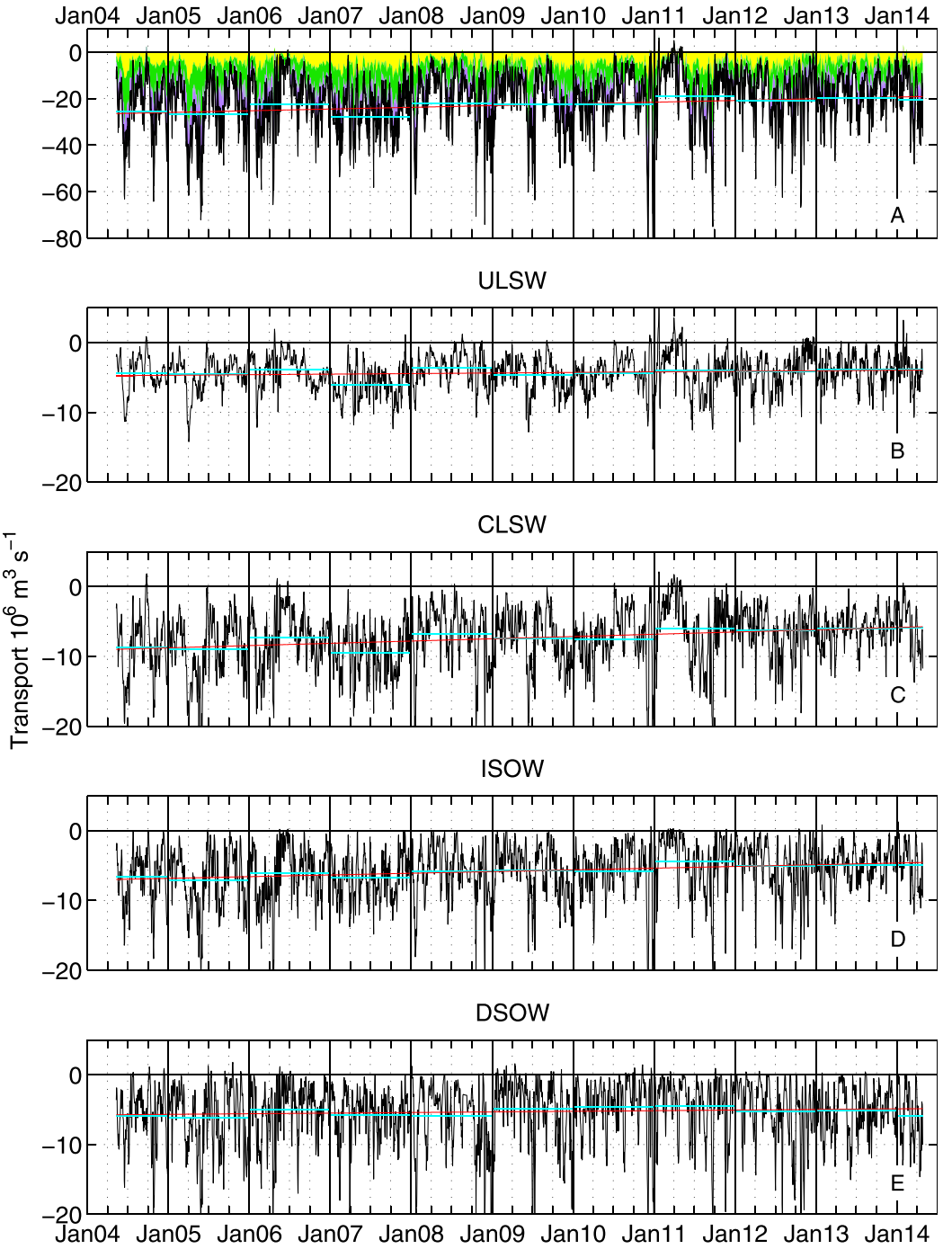

Figure 5. Time series of DWBC transport at Line W partitioned by water mass. Negative values correspond to equatorward flow. Total intermediate and deep water transport is given in (a) with each layer's contribution to the total identified by color (ULSW = yellow, CLSW = green, ISOW = purple, and DSOW = black). The individual layer transport time series: (b) ULSW, (c) CLSW, (d) ISOW, and (e) DSOW, respectively. As described in the text, values each day for each layer represent the most southward value of the transport stream function integrated to mooring W5. The red lines are linear least square fits to the transport estimates versus time. To facilitate comparison with sustained measurement programs that report annual-mean transports, cyan lines mark the calendar-year averages of the Line W estimates.

mean. Taking the CLSW layer as example, a time series of layer-thickness was constructed by averaging the daily estimates from those moorings in the equatorward DWBC flow each day, and a corresponding width series was developed by dividing daily layer area estimates by these thickness data. Layer-averaged velocity was determined from the ratio of transport estimates to area estimates. The decomposed transport series has

7 time-varying components. The term that contributes the most to the CLSW transport variance (by more than a factor of 2 over the second largest term) is $<H><W>V'$: transport variance due to fluctuations in the layer-averaged velocity. The next largest contributor to transport variance is the $<H>W'<V>$ term. This is the case for the daily time series as well as that after low-pass filtering each of the terms over a 6 month period. It is only on still longer time scales, as represented by 10 year linear least square fits to the transport contributions, that layer-thickness variations contribute significantly to transport variance (becoming the second largest contributor to the decadal trend after that due to layer-average velocity change).

High coherence ($\geq$0.8) is calculated between pairs of adjacent layer transport series for frequencies below 0.1 cpd. This is consistent with the cross-line, subinertial velocity fluctuations being strongly barotropic in the Slope Water, particularly below ~500 m depth. Supporting this characterization is the leading empirical orthogonal mode of the subinertial velocity profile variability at W3 (that accounts for approximately 80% of the variance at this site) that is single signed in depth with surface intensified amplitude that decays to less than 20% of the surface value by 1000 m depth, and then maintains this amplitude to the bottom (not shown). In addition, fluctuations in the width of the DWBC are similar in each of the layers. Weak shear at depth and similar layer-widths combine to yield the observed correlated variability in DWBC layer transports.

Time-average transports over the 10 year observing period based on the daily estimates, Table 2, are larger than those based on the Eulerian-mean flow field, as was seen previously in the first 4 years of the measurement program. The difference is in part due to the shoreward influence of Gulf Stream meandering on the Eulerian-mean field that is evident by comparing Figures 2 and 4. The statistical uncertainty of these mean transport values given in the table were derived in terms of the estimated decorrelation times (twice the integral time scales). A bootstrap uncertainty estimate procedure returned smaller error bars—the difference possibly because the transport estimates are not normally distributed. Based on these error bars, the 10 year-averaged daily layer transports reported here are marginally smaller than the corresponding averages over the 2004–2008 period reported by *Toole et al*. [2011], manifesting long-term trends in the DWBC flow, see below. Less straightforward is assessing uncertainty associated with the finite width of the moored array. Indeed, short of physically extending the array to the opposite coast, as is done at 26.5°N by the Rapid/Mocha program [*Cunningham et al*., 2007] or synthesizing the same [e.g., *Willis*, 2010], one cannot be sure at any given time if the array is spatially aliased or not (i.e., is only measuring one side of a recirculating eddy at the offshore end of the array). Two such physical processes potentially influencing the Line W transport estimates are discussed below.

5. Modes of Subinertial Transport Variability at Line W

5.1. Synoptic Scale

A host of physical mechanisms induce DWBC variability at Line W including internal gravity waves [e.g., *Silverthorne and Toole*, 2008; *Joyce et al*., 2013] and Topographic Rossby Waves [e.g., *Thompson*, 1971; *Fratantoni and Pickart*, 2003; *Peña-Molino et al*., 2012]. Two somewhat longer-period modes of variability are explored here: Gulf Stream meanders and Warm Core Rings. Noted earlier were the studies by *Savidge and Bane* [1999a,1999b] and *Andres et al*. [2016, 2017] that implicated vortex stretching at times of offshore displacements of the baroclinic Gulf Stream as being responsible for the spin up of deep cyclones. Investigating further, a composite section of moored velocity at times of offshore Stream displacements was constructed with guidance again provided by the altimeter-based surface geostrophic velocity data. Mooring data from days when the surface velocity core of the Gulf Stream was south of 37.3°N (Figure 3), and the Slope Water surface velocities were between 0.1 m/s poleward and 0.3 m/s equatorward (to exclude times when Warm Core Rings and other strong anomalies were present) were identified and averaged, Figure 6. At W6 (whose record does not span the full 10 years), strong equatorward flow is observed below ~700 dbar at times of southward Gulf Stream displacement (reaching nearly 20 cm/s in this composite average). The vortex in the corresponding composite average based on shipboard measurements [*Andres et al*., 2017, Figure 4], appears more barotropic in its equatorward limb but is otherwise quite similar. (Recall that the upper ocean velocities at W6 are interpolations between altimeter-based surface geostrophic currents and subsurface current meter records from ~500 m depth whereas the ship measurements were direct.) The principle Gulf Stream flow was seaward of the array at these times and so is largely not imaged in this composite.

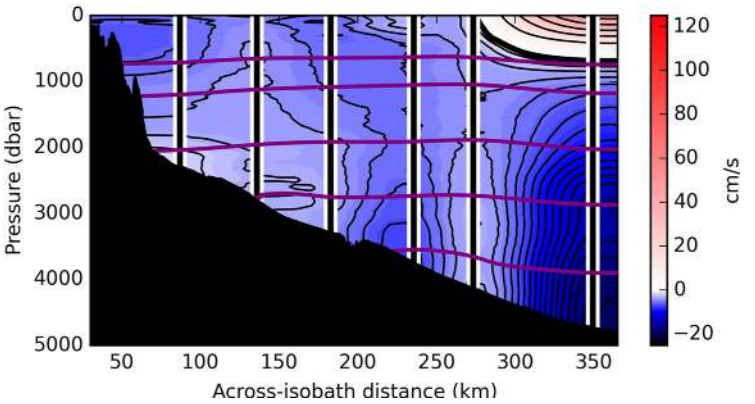

Figure 6. Composite Line W across-line velocity section constructed from observations on days when the Gulf Stream velocity core was displaced south of its mean location and there were no strong surface velocity anomalies present in the Slope Water. Contour interval is 1 cm/s for equatorward flows and 10 cm/s for poleward velocities; the thick black line marks the zero isotach.

We believe this strong equatorward flow seen in Figure 6 derives from the shoreward half of cyclonic vortices associated with southward meanders of the Stream and as such does not represent a net transport across the latitude of the Line W array. These deep cyclones appear not to extend shoreward to W5 in this sample subset and indeed, the mean velocity field over the shallower moorings looks very similar to the ideal-case composite. Based on this evidence, we decided to report DWBC transports in Figure 5 and Table 2 evaluated across moorings W1–W5. In similar vein, we believe the 10 year Eulerian-mean transport estimates integrated to W6 given parenthetically in Table 2 are spatially aliased. Interestingly, a composite mean velocity section constructed from moored profiles at times when the Gulf Stream was displaced north of its mean latitude (not shown) was not the opposite of Figure 6 (i.e., there was no indication of a deep anticyclonic eddy feature in that composite). Perhaps the vortex stretching/squashing mechanism that has been invoked to explain the deep cyclones manifests differently over the more steeply sloping bathymetry inshore of W5 than the flatter bathymetry at and south of W6.

Anticyclonic Gulf Stream Warm Core Rings (WCRs) constitute the other major class of DWBC disturbances at Line W. These cutoff northward meanders of the Stream commonly form east of Line W and drift southwest through the Slope Waters, eventually coalescing back with the Stream [*Brown et al.*, 1986]. Brown et al.'s analysis indicated that WCRs typically form east of 70°W and only a small subset drift as far southwest to encounter Line W (i.e., most are entrained into the Gulf Stream to the east of Line W). However, the meander character of the Stream appears to have evolved of late with meandering occurring more frequently and/or energetically to the west [*Andres*, 2016]. Again we turn to the record of altimeter-estimated across-line surface velocity extrema, this time to identify times when WCRs were present on Line W. Associating days when surface velocity anomalies north of the North Wall were greater than 50 cm/s with occurrences of WCRs yielded a total of 214 days out of the 10 year Line W record (6% of the time) when WCRs impacted the array (Figure 3).

Rings can impact our transport estimates in two ways; the first is kinematic. The azimuthal flow of a WCR would bias our DWBC transport estimates if the Ring edge extended offshore of W5. This appears to have occurred 7 times over the 10 years. Excluding these periods from the 10 year-mean DWBC transport estimates had negligible impact on the time-mean transport estimates. But WCRs also impact the spatial structure of the mean velocity field sampled by the moored array, as was previously documented by *Flagg et al.* [2006] in the *Oleander* data set (see http://po.msrc.sunysb.edu/Oleander/ and http://www.po.gso.uri.edu/rafos/research/ole/index.html). Averaging the 4% of the W1 daily velocity profiles when the poleward surface velocity was greater than 30 cm/s (Figure 3, interpreted as days when a WCR was influencing the flow at this mooring) yields the profile in Figure 7 that has monotonically increasing poleward velocity above 1500 dbar, reaching more than 50 cm/s at the surface. Adopting the WCR occurrence rate of 4%, a weighted-average velocity profile constructed from the ideal composite profile at W1 (weight of 0.96) and this WCR profile (weight of 0.04) is similar to the full 10 year Eulerian mean in that it exhibits a weak local maximum in equatorward flow around 500 m depth (Figure 7). So while it might be tempting to attribute the Eulearian-mean middepth velocity core in the DWBC at W1 to enhanced flow of Labrador Sea Water, this weighted averaging exercise suggests the mean velocity core may simply be a consequence of occasional surface intensified WCR flow. That said, water property tracers are advected by the total ocean flow without regard to the dynamics of those motions. If this superposition of

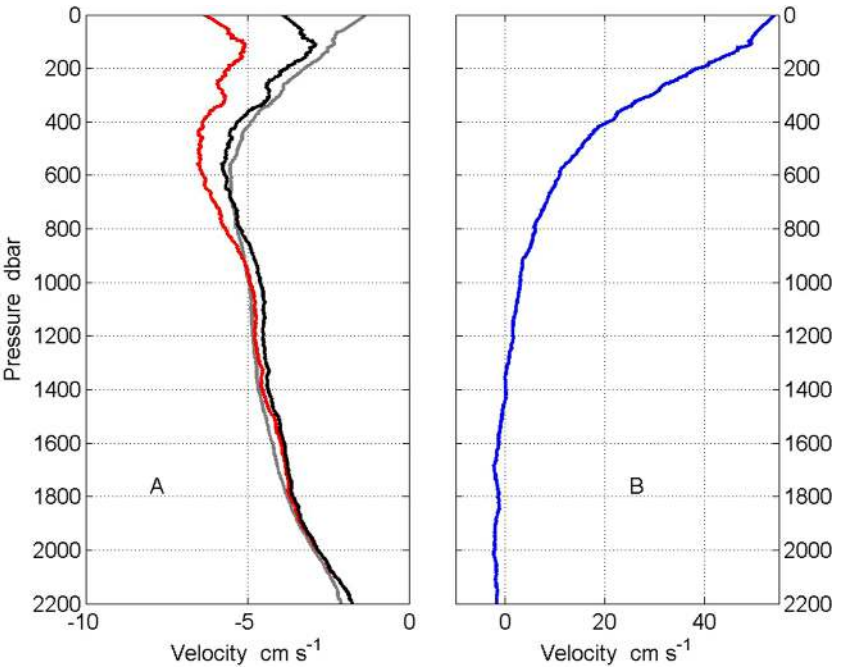

Figure 7. Composite-average Mooring W1 across-line velocity profiles (positive directed to the northeast) based on data (a) when the flow field was in an ideal configuration (red) and (b) from times when Gulf Stream Warm Core Rings were positioned over the array (blue). The black curve in Figure 7a is the across-line velocity profile for the full 10 year average while the gray curve is the weighted average of Ring and ideal state profiles as discussed in the text.

generally weak equatorward drift with occasional surface intensified WRC flow as seen at W1 is replicated along the shelf break to the north, one should expect a middepth water property core co-located with a middepth Eulerian-mean equatorward velocity extremum, as is observed at Line W in, for example, salinity, dissolved oxygen and CFCs [*Joyce et al*., 2005; *Toole et al*., 2011; *Le Bras et al*., 2017]. But farther offshore, the water property anomalies of the WCRs will complicate this simple kinematic description.

5.2. Decadal Trends

Looking on longer time scales, the Line W DWBC transport time series of Figure 5 hint at a long-term trend of (or decadal-time-scale oscillation phased to give) decreasing equatorward flow over the measurement period. To quantify this indication, linear least square trend estimates for the intermediate and overflow layer transports were obtained together with statistical uncertainty estimates (Figure 5 and Table 2). Confidence bounds were obtained both from a bootstrap procedure (derived from the distribution of trend estimates obtained from repeated subsampling of the transport data with replacement and linear least square fitting) and the theoretical uncertainty based on estimated degrees of freedom. (We report in Table 2 values from the bootstrap procedure which were the larger of the two respective estimates.) Statistically significant trends of decreasing equatorward transport are obtained for the CLSW, ISOW, and DSOW layers as well as the four-layer summed transport. Of these, the trend in CLSW transport is the greatest; the overall linear fit returns a transport of -9.0×10^6 m^3/s at the beginning of the field program that falls to -5.8×10^6 m^3/s at its end. While some of the CLSW transport decrease is attributable to thinning of this layer over time [*Le Bras et al*., 2017], approximately 75% of the decadal trend in CLSW transport is the result of a reduction in layer-area-averaged equatorward velocity. Statistically significant weakening trends are also obtained for the overflow layers, again principally due to changes in layer-averaged velocity. The corresponding linear fit to the combined Labrador Sea and Overflow Water DWBC transport decreases from 26.4×10^6 to 19.1×10^6 m^3/s through the Line W observing period. Similar trends in DWBC transport are obtained from a combined analysis of Line W shipboard and moored observations (T. Joyce, personal communication, 2017). In contrast, we find no significant trend in upper ocean Slope Water transport. The linear fit to the total equatorward boundary current transport (the five-layer sum of Table 2) fell from 33.3×10^6 m^3/s in spring 2004

to 25.9 $\times$ 10^6 m^3/s in spring 2014 (all due to change in the intermediate and, to a lesser extent, deep water flow).

No significant linear trends with time are seen in the width of these equatorward-directed layers over the Line W period. The coarse spatial resolution of the moored array (and adopted transport estimation procedure) could easily mask a small, long-term signal. A weak southward trend with time of just over 1 km/yr is observed in the latitude of the North Wall at Line W inferred from altimeter data. The sense of this trend, if extended down to the intermediate and deep waters at Line W, is of the wrong sense to account for weakening equatorward DWBC transport with time. (A southward shift of the Gulf Stream results in a wider DWBC and more transport if the layer-averaged velocity is constant.) However, we note that regional meridional shifts in the Gulf Stream have been reported [e.g., *Joyce et al*., 2000; *Pérez-Hernández and Joyce*, 2014; *Davis et al*., 2017] that are not always identifiable locally. In particular, these latter papers document a regional northward shift in the Gulf Stream path during the Line W field program. How regional shifts of the Gulf Stream might influence DWBC flow is still unclear, though *Le Bras* [2017] explores some possible sensitivities relating to flow instability and eddy exchanges.

6. Transport Comparisons

Long time series of DWBC and/or AMOC transport have been reported for various latitudes in the North Atlantic. Here we make comparisons to some of those other transport estimates using consistent layer definitions as much as is practical. For Line W, we focus on the 10 year averages of the daily DWBC transport estimates as we believe these most accurately document the mean DWBC meridional transports across Line W for the 2004–2014 period. But as some of the published mean DWBC transport estimates are based on Eulerian averages, we present both for Line W in Table 2. We begin with North Atlantic DWBC observations from other latitudes, proceed to discuss some Atlantic-wide net meridional transport estimates and end with comparisons to some state estimate model results.

Investigators from the GEOMAR Helmholtz Centre for Ocean Research have maintained a moored array near 53°N at the "exit of the Labrador Sea" for nearly 20 years now (1996 to the present) [*Zantopp et al*., 2017, and earlier references given therein]. These authors report a DWBC time-mean meridional transport of 30.2 $\pm$ 6.6 $\times$ 10^6 m^3/s of North Atlantic Deep Water (integrating vertically between 400 m and the bottom using techniques very similar to those employed here—i.e., integrating synoptic velocity estimates laterally to zero crossings of the boundary current flow, then averaging). Using potential density relative to 2000 dbar (σ_2) to subdivide the water column, Zantopp et al. find a near equipartitioning of mean transport between Labrador Sea Water (14.5 $\pm$ 3.8 $\times$ 10^6 m^3/s, integrating between 400 m and $\sigma_2 = 36.95$ kg/m^3) and Lower North Atlantic Deep Water (15.8 $\pm$ 3.8 $\times$ 10^6 m^3/s, integrating between $\sigma_2 = 36.95$ kg/m^3 and the bottom). Taking Line W daily profiles from W3, the mean neutral density at $\sigma_2 = 36.95$ kg/m^3 is 27.8936 kg/m^3 (with a standard deviation of 9.7 $\times$ 10^{-5} kg/m^3). Thus, the Zantopp et al. bounding isopycnal between intermediate and deep waters is effectively the boundary between CLSW and ISOW in the present analysis. Similarly, the 400 m top bounding surface chosen by Zantopp et al. appears reasonably close to the 27.68 kg/m^3 σ_θ (potential density relative to 0 dbar) contour drawn on their Figure 4. This σ_θ surface at W3 equates to $\gamma_n = 27.8025$ kg/m^3 (with standard deviation of 0.0026 kg/m^3—which is close to the upper bounding neutral density for ULSW at Line W). Thus, to a close approximation, the Zantopp et al. partitioned transport estimates may be directly compared to the merged layer transports at Line W reported here. Summing over layers, the average of the daily Line W Labrador Sea Water transport values is $-11.71 \pm 0.8 \times 10^6$ m^3/s and of the Overflow Waters is $-11.06 \pm 0.67 \times 10^6$ m^3/s (95% confidence bounds given). It thus appears that the Line W mean transport estimates for these summed layers are somewhat smaller than those estimated at 53°N (but we note that the uncertainty bounds of the respective estimates overlap). With their longer record, Zantopp et al. find evidence of decadal-time-scale oscillations in the DWBC Overflow Water transport at 53°N. No obvious correlated signal is seen in the corresponding (but shorter duration) Line W transport data.

Moving south, *Mertens et al*. [2014] presented an assessment of DWBC and North Atlantic Current (NAC) flow across 47°N (east of Flemish Cap) based on 2 years of mooring data (2009–2011) and seven hydrographic sections occupied between 2003 and 2011, together with satellite altimeter data and output from an eddy-resolving model. Based on the shipboard data, these authors report an average equatorward

transport below $\sigma_\theta = 27.68$ kg/m^3 of $31.8 \pm 3.6 \times 10^6$ m^3/s, roughly equipartitioned between velocity cores over the continental slope and rise. Analysis of the 2 year moored array yielded a mean transport estimate for the former of 16.3×10^6 m^3/s with a reported standard deviation of 4.0×10^6 m^3/s. As noted earlier, the top bounding isopycnal chosen by Mertens et al. is effectively that used by *Zantopp et al*. [2017] and yields a comparable time-averaged DWBC transport. The length of the in situ record from this latitude is too short to assess interannual trends or oscillations; analysis of model output by these investigators found little temporal variation in the transport of the slope core but sizable interannual oscillations in the net equatorward flow inshore of the NAC, a significant fraction of which was said to recirculate back to the north.

In similar fashion to the study at 53°N, investigators from the Bedford Institute of Oceanography and later from GEOMAR Kiel maintained a DWBC moored array southeast of Grand Banks near 42°N [*Clarke et al*., 1998; *Schott et al*., 2004, 2006; *Schott and Brandt*, 2007]. In this latter work, time-averaged DWBC transport in 2 year segments (1993–1995; 1999–2001; 2003–2005) were reported for waters below the $\sigma_\theta = 27.74$ kg/m^3 surface (again by lateral integration of the synoptic velocity field realizations and then averaging). These average DWBC transport estimates were indistinguishable from one another: $-11.3 \pm 1.1 \times 10^6$, $-11.2 \pm 0.9 \times 10^6$, and $-11.8 \pm 1.0 \times 10^6$ m^3/s. Again referencing to mooring W3, the $\sigma_\theta = 27.74$ kg/m^3 surface equates with $\gamma_n = 27.8774$ kg/m^3 (with standard deviation of 0.0025 kg/m^3) which on average lies just 100 m above the present study's boundary between ULSW and CLSW. Ignoring this small difference in bounding surface depth, the mean Line W daily transports summed over the CLSW, ISOW, and DSOW layers yields a time-average figure of $-18.4 \pm 1.61 \times 10^6$ m^3/s that may be compared directly to the estimates from 42°N. Accepting these figures at face value suggests somewhat larger DWBC transport at 53°N, 47°N and Line W than at Grand Banks where the boundary current is narrowly constrained between the North Atlantic Current and the Bank. This may imply existence of significant local recirculations at 53°N and 47°N, a somewhat weaker one at Line W and absence of much local recirculation at Grand Banks.

At 26.5°N, a DWBC moored array was maintained east of Abaco between 1986 and 1997 [*Lee et al*., 1990, 1996; *Bryden et al*., 2005]. These latter authors estimate an Eulerian-time-mean equatorward DWBC transport below 1000 m of 34.6×10^6 m^3/s with a statistical uncertainty of 3.7×10^6 m^3/s and up to 4×10^6 m^3/s of uncertainty from methodology. No density information was reported. These authors rationalized the large boundary current transport by citing a broad, diffuse northward recirculation between the offshore edge of the DWBC and the Mid-Atlantic Ridge.

Turning to AMOC net transport estimates, *Willis* [2010] synthesized a time series of net upper limb AMOC transport about 41°N by combining Argo float data and satellite altimetry. For the 2004–2006 period, he obtains a figure for mean net poleward transport above 1130 m of $15.5 \pm 2.4 \times 10^6$ m^3/s and no significant trend with time in an altimeter-only transport proxy over the 2002–2009 period. Invoking mass balance, one might expect a similar-sized mean equatorward return transport at depth. Willis' integration depth of 1130 m is close to the depth of our bounding isopycnal between ULSW and CLSW and so one might roughly compare the negative of Willis' figure to our combined CLSW and the Overflow Layers transport (mean of $18.4 \pm 1.6 \times 10^6$ m^3/s). Statistical agreement of the respective estimates is evident, but we note that Argo float density is rather poor within western boundary currents owing to fast flow speeds so it is unclear how representative Willis' mean dynamic height profile at the western boundary is of the true time-averaged profile. More generally, we are unsure how to compare horizontally integrated transports to those within density layers at latitudes north of Cape Hatteras where the Gulf Stream is separated from the coast (and water mass layers vary greatly in depth across the basin).

Measurements about 26.5°N latitude were expanded to full basin width beginning in 2004 under the joint U.K.-U.S. RAPID/MOCHA program to obtain basin-wide AMOC observations [e.g., *Cunningham et al*., 2007; *McCarthy et al*., 2015; *Srokosz and Bryden*, 2015]. Owing to the observational methodology that employs dynamic height moorings to derive horizontally averaged velocity profiles via the geostrophic thermal wind balance, RAPID/MOCHA volume transport estimates have been reported in depth space rather than isopycnal coordinates. Using temperature and salinity data from western-boundary moorings WB2 and WBH2 (26°28.9′N, 76°37.5′W; 26°30.8′N, 76°44.3′W, respectively) to characterize the depths of neutral density surfaces across the basin, D. Smeed (personal communication, 2017) derived time-averaged net meridional layer transport estimates for the period April 2004 to October 2015 for comparison with Line W, Table 2. Similarity between a time-averaged net meridional layer transport at 26.5°N and the corresponding Line W DWBC mean layer transport implies relatively small recirculation transport of those waters at Line W. Net AMOC

transport at 26.5°N varies on a host of time scales. Notably, *Smeed et al*. [2014] report a decreasing trend to the AMOC from the RAPID/MOCHA observations of 7%/yr, punctuated by a dramatic dip of 30% in the 2010–2011 time period [*McCarthy et al*., 2012, *Bryden et al*., 2014]. While tempting to equate this long-term trend with the decrease in Line W DWBC transport reported here, the Line W transport trend was greatest in the intermediate waters whereas the decrease in net meridional flow at RAPID is more focused in the deep waters (Smeed, personal communication, 2017). Moreover, temporal change in ocean layer volumes between observing latitudes (storage change) can be significant and easily confound such comparisons [*Yang*, 2015; *Zou and Lozier*, 2016; *Evans et al*., 2017].

Still farther south but in similar vein, time series estimates of the AMOC cold limb transport have been made at 16°N between Guadaloupe and the Mid-Atlantic Ridge since early 2000 [*Kanzow et al*., 2006; *Send et al*., 2011]. Similar to 26.5°N, the DWBC at 16°N is augmented by a strong recirculation that spans much of the Guiana Basin west of the Mid-Atlantic Ridge (McCartney, see http://www.whoi.edu/page.do?pid=30759). The MOVE array data are analyzed to obtain estimates of the net equatorward deep water transport below 1200 m (relative to 4950 m). Taking these estimates from the MOVE project website—http://mooring.ucsd.edu/index.html?/projects/move/move_results.html, we compute a mean meridional transport over the Line W period of -23.5×10^6 m^3/s (with a standard deviation of 4.1×10^6 m^3/s). M. Lankhorst (personal communication, 2017) reports that the mean potential density anomaly at 1200 m on the MOVE line is 27.65 kg/m^3 (varying by 0.07 between the eastern and western ends of the array). This potential density figure translates to $\gamma_n = 27.769$ kg/m^{3}at W3, which is again close to our bounding neutral density at the top of the ULSW layer. Summing over layers as before, we find that the MOVE mean transport estimate is statistically indistinguishable from the summed mean transport of Labrador Sea and Overflow Waters at Line W (Table 2). Integrating laterally over the DWBC and recirculation, the net equatorward AMOC limb at 16°N appeared to have decreased in strength by 20% over the 2000–2009 period [*Send et al*., 2011], but the more recent observations suggest a strengthening (see the MOVE website cited above). Here again the complicating variable when comparing transport variations between latitudes is changes in water mass storage.

Beyond direct analyses of field observations, a final round of transport comparisons were made with output from the ECCO (Estimating the Circulation and Climate of the Ocean) v4, release three state estimate [*Forget et al*., 2015, 2016; C. Wunsch, personal communication, 2017]. Time-averaged transport for the intermediate and deep water layers defined at Line W were estimated from monthly mean model fields along 40°N, chosen as being geographically representative of the Line W region, Table 2. (On basin scale, the depths of our bounding isopycnals in the model appeared reasonable, although issues with T/S properties have been reported previously for these types of state estimates [e.g., *Koehl*, 2015].) We calculated an average net transport for the waters with γ_n between 27.8 and 28.125 kg/m^3 in the ECCO v4r3 output over the Line W measurement period of -13.8×10^6 m^3/s, but the spatial distribution of this deep meridional transport is odd. More than half of the time-averaged equatorward deep water flow in this state estimate is located east of 40°W with enhanced flows on both flanks of the Mid-Atlantic Ridge, while the Labrador Sea Water layers over the American continental slope flow north in the mean with an unrealistically broad Gulf Stream. (Poor representation of the Gulf Stream separation at Cape Hatteras is a common feature of coarse resolution models; ECCO would seem to be no exception.) For this most recent release of the state estimate, a linear least squares fit to the net sum of intermediate and deep water meridional transport over the Line W period falls from -15.0×10^6 to -12.6×10^6 m^3/s. This is in the same sense but much weaker than the Line W DWBC transport decrease over this period. Poor representation in ECCO of the flow field about the western boundary complicates interpretation of the differences with the Line W observations.

In an independent study, *Jackson et al*. [2016] report AMOC temporal anomalies diagnosed from the GloSea5 reanalysis product. At 45°N (closest latitude to Line W discussed in the paper), a decrease in net geostrophic AMOC strength of around 2×10^6 m^3/s over the Line W study period was found in the model. No information about the time-averaged AMOC or zonal distribution of the flow anomalies in GloSea5 were presented. A consistency diagnosis of water column density also discussed in this paper suggested this AMOC slowdown was related to a buoyancy increase at the western boundary that in turn was tied to changes in subpolar water mass transformation. (As the geostrophic thermal wind relation is not causal, one cannot say that the change in density *caused* the change in AMOC or vice versa.) Pursuing this diagnostic, annual averages of water column density at the western boundary were calculated for 2004 and 2014 at

Line W and found to have decreased by 0.02 kg/m^3 between ~500 and 2000 m (similar to what Jackson et al. show in their Figure 4).

7. Discussion

Comparing the time-averaged transport estimates reviewed in section 6, a roughly consistent picture is starting to emerge of the Atlantic's time-average DWBC and AMOC. Some 15 $\times$ 10^6 m^3/s of Atlantic intermediate (ULSW and CLSW) and deep (ISOW and DSOW) water are carried equatorward by the DWBC in the northern hemisphere, with local recirculations significantly augmenting the boundary current flow at 53°N, 26.5°N, and 16°N and to a lesser extent at Line W. There appears to be little local recirculation at 42°N. One surprising aspect to the comparisons reviewed above is how similar some of the Line W layer mean DWBC transport estimates are to the corresponding mean net (boundary to boundary) equatorward deep water transport estimates at 26.5°N and 16°N. Deep circulation theory [e.g., *Stommel*, 1957] and existence of eddy-driven recirculations would both argue that the DWBC transport should exceed the net meridional transport in the cold limb of the AMOC. That appears to be true at 26.5°N and 16°N, but we presently lack for comparison accurate, water-mass-partitioned, basin-wide-integrated net transport estimates at the latitudes of the northerly DWBC arrays. Unfortunately state estimate models appear not as yet able to shed light on the detailed nature of the North Atlantic DWBC and spatial structure of the time-average AMOC flow.

A decreasing equatorward flux of the denser mode of Labrador Sea Water over the Line W measurement period is perhaps not unexpected given the slackened water mass transformations by winter convection in the Labrador Sea since the early 1990's [*Yashayaev and Loder*, 2016] and finite time for anomalies to move from the subpolar to subtropical Atlantic [e.g., *Rhein et al*., 2015; *Smith et al*., 2016; *Le Bras et al*., 2017]. We find no compensating increase in the transport of lighter LSW modes that might be anticipated if total intermediate water production were steady and only the density of the end product was varying. Moreover, we saw no evidence at Line W of the recent strengthened Labrador Sea Water mass transformations reported by *Yashayaev and Loder* [2016]. Line W ended before we could expect passive water property anomalies associated with renewed deep convection to have reached that latitude [*Le Bras et al*., 2017]. But transport anomaly signals may propagate equatorward at much faster speed than (passive) water property anomalies. The Line W data also suggest a weakening of the DWBC transport of Overflow Waters. However sustained observations of the Denmark Strait and Faeroe Bank overflow transports have found no long-term trends [*Jochumsen et al*., 2012; *Hansen et al*., 2016]. The large transport variability induced by Gulf Stream meandering, Rings, waves and other high-frequency motions make it difficult to characterize and assign attribution to small-amplitude variations in DWBC volume transport at that site. But multidecadal-length records of AMOC components are now becoming available from various places around the basin. With long records it becomes possible to filter out higher-frequency signals and detect small-amplitude, long-period changes. While synthesis of these observations into an internally consistent dynamical description of AMOC variability has not as yet been accomplished, we look forward to a time when this will be possible.

Appendix A: Moored Array Data Return and Processing

The Line W moored array was designed to sample the intermediate and deep waters over the continental slope underlying Topex-Poseiden altimeter track number 126 extending from Cape Cod towards Bermuda (see Figure 1). Data return from the Line W moored instruments was reasonably good but not perfect, Figure A1. As outlined in the following, significant effort went into deriving the daily profiles of subinertial temperature, salinity and velocity that are analyzed here. The individual moorings in the array were designated W1 through W6—Table A1. The array configuration for the first 4 years of the field program consisted of Moored Profiler moorings at sites W1, W3, and W5 with fixed-depth sensors on W2 and W4 (the latter are referred to here as "conventional moorings"). These Moored Profiler moorings were serviced on annual basis while the conventional moorings were designed for 2 year deployments. A WHOI-supported initiative attempted two conventional mooring deployments at W6 during this period, but neither returned much usable data. In 2008 the array was reconfigured with conventional moorings deployed at sites W1, W3, W5, and W6 and Moored Profiler moorings at W2 and W4. Bad weather during two cruises in 2008 prevented timely renewal of all of the moorings in the array, resulting in some extended data gaps when batteries in

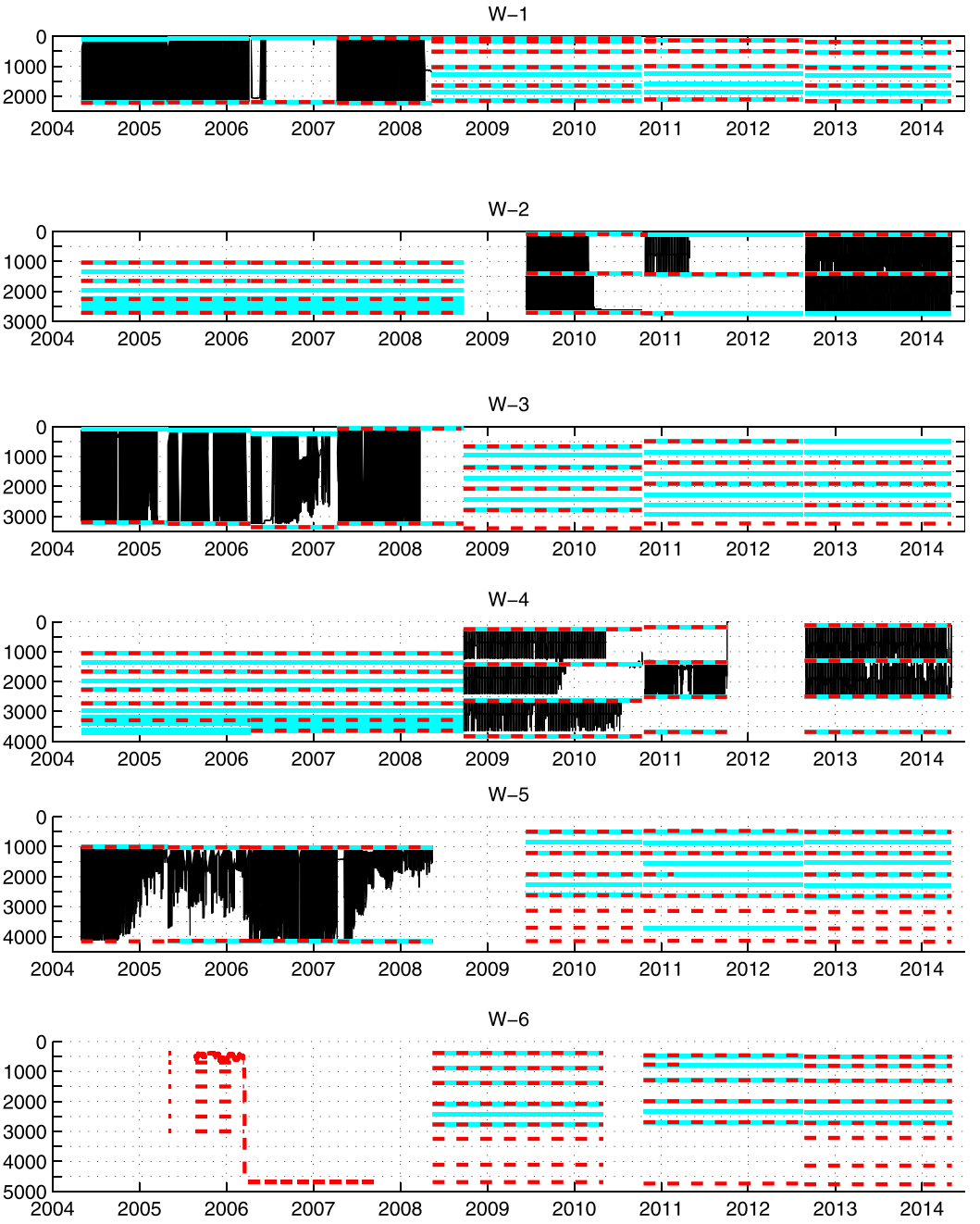

Figure A1. Graphical presentation of the moored sensor performance during the Line W program. For each mooring site, the times and depths when good data were obtained from Moored Profilers (black lines), fixed-depth current meters (red broken lines), and fixed-depth temperature-conductivity (or temperature-conductivity-pressure sensors—cyan lines) are shown. In each case, the abscissa spans the period of the full Line W moored program and the ordinate is pressure (with axis length scaled according to mooring site depth).

the deployed instruments were exhausted. Also, the W4 mooring deployed in late summer 2011 was lost in its entirety.

Subsurface mooring technology was used exclusively with the shallowest measurement level ranging between 50 and 1000 m depending on mooring site and setting (the shorter moorings reflecting the program's focus on intermediate and deep waters). The conventional moorings supported current meters typically logging 15 or 30 min averages and temperature-conductivity or conductivity-temperature-depth sensors taking samples every 15 min. Vector-Averaging Current Meters (VACMs) were used extensively on Line W but in the later years of the program, Nortek Aquadopp, Nobska MAVS, and Aanderraa RCM-11

Table A1. The Line W Moored Array[a]

Mooring	Latitude	Longitude	Bottom Depth (m)	Mooring Style	Shallowest Sensor (m)
W1	39°36.32′N	69°43.62′W	2238	MMP: 2004–2008	48–85
				Conventional: 2008–2014	62–177
W2	39°13.54′N	69°26.73′W	2752	Conventional: 2004–2008	1026–1033
				MMP: 2008–2014	76–98
W3	38°50.33′N	69°10.63′W	3248	MMP: 2004–2008	95–170
				Conventional: 2008–2014	480–650
W4	38°26.27′N	68°53.87′W	3686	Conventional: 2004–2008	1040
				MMP: 2008–2014	100–222
W5	38°5.80′N	68°38.95′W	4110	MMP: 2004–2008	988–1010
				Conventional: 2008–2014	479–492
W6	37°28.66′N	68°18.34′W	4700	Conventional: 2008–2014	268–438

[a]Observations from these sites between 11 May 2004 and 27 April 2014 are analyzed here. Average mooring locations and corresponding ocean depths are given along with the type of mooring deployed: MMP indicates a mooring that supported a McLane Moored Profiler while a Conventional Mooring supported discrete current meters and T-C/CTD sensors. The shallowest sensor column gives the range of depths for the various settings of each mooring of that style.

current meters were also utilized as the WHOI inventory of VACMs was phased out. Sea-Bird Electronics, Inc. SBE 37-SM MicroCAT sensors were used, a subset with the optional pressure channel. Line W represented the first long-term operational deployments of the McLane Moored Profiler (MMP, http://mclanelabs.com/mclane-moored-profiler/) and as such, revealed instrumental and procedural shortcomings that over time led to improvements in the technology and protocols. During the first phase of the Line W array, single MMPs were fitted to moorings with fixed sensors above and below the profiling span. In the second phase of the array in order to extend the functional endurance of the Moored Profiler moorings to 2 years, multiple MMPs were mounted on W2 and W4 with fixed sensors between each profiled segment. The MMPs were most commonly programmed to collect bursts of 4 one-way profiles at specified interval—typically every fifth day—with the profiling synchronized between the MMP moorings. Within each burst, profiles were initiated every 9.3 h, which is approximately half the local inertial period at Line W and 3/4ths the M2 semidiurnal tidal period. Consequently, averaging the four profiles in a burst effectively filtered near-inertial and tidal signals, yielding an estimate of the subinertial flow and stratification variability [*Silverthorne and Toole*, 2008]. In addition to burst profiling, the MMPs deployed in phase 2 were programmed to park midspan between bursts and sample for 5 min each hour, replicating the data obtained from a fixed-depth current meter/MicroCAT pair (albeit at much slower sampling rate).

The T-C and CTD sensors were routinely calibrated in the laboratory between deployments (both the MicroCATs and the sensors on the MMPs), as were the thermistors in the VACMs. No subsequent adjustments were made to the temperature and pressure observations. Time-variable conductivity calibration adjustments were subsequently derived based on (water-sample-calibrated) ship CTD station data about each mooring and assumed stability of the deep ocean potential temperature-salinity relationship. Special effort was made to ensure salinity profile consistency across the multiple MMPs on the phase 2 moorings.

Fixed-sensor records were processed and archived at their native sample rate and for those instruments that did not include a pressure sensor, pressure time series were synthesized based on the available pressure records from other levels on each mooring. The temperature, salinity and velocity time series data were low-pass filtered (36 h cutoff), decimated to 1 day intervals, then spline interpolated in pressure to 2 dbar resolution. Neutral density [*Jackett and McDougall*, 1997] was subsequently estimated at each grid point.

The MMP profile data were processed to 2 dbar resolution using custom analysis routines and when necessary, interpolated vertically over the designed profile span using the available contemporaneous fixed-depth data from each mooring and past and/or following observations. (Figure A1 documents when extrapolation was required.) Most commonly, vertical gaps in velocity profiles were filled by linear interpolation while missing temperature and salinity data were synthesized using near-contemporaneous full profiles and available fixed-sensor data while preserving temperature-salinity correlation. The extended full profiles in each burst were subsequently averaged to obtain subinertial data as noted above and neutral density calculated. Daily profile estimates were then derived by interpolation in time, with guidance provided by the fixed-sensor data on each MMP mooring. Inherent in those procedures was the assumption that the subinertial variability on few-day periods has large-vertical scale and so definable by the available fixed-depth observations (verified by the heavily instrumented conventional mooring data).

Although the array was focused on intermediate and deep water signals, for completeness, the subinertial mooring data were extended vertically to the surface. Daily gridded surface geostrophic velocity estimates produced by Ssalto/Duacs and distributed by AVISO with support from CNES (http://www.aviso.altimetry.fr/duacs/) were mapped to each mooring site. Velocity was then vertically interpolated on each day between the surface and the shallowest moored estimate. Analysis of the handful of upward-looking Acoustic Doppler Current Profiler records from Line W moorings indicated that the altimeter-derived surface geostrophic velocities were highly coherent with the directly measured near-surface flow on time scales longer than ~20–30 days. Temperature and salinity data were extrapolated upwards under the assumption that the variability at a given depth was chiefly due to vertical displacement. For each day of each mooring record, time-varying reference temperature and salinity profiles derived from adjacent mooring or shipboard station data close in time were shifted vertically to match the observations at the top of the mooring. Although not yielding particularly realistic T and S information in the upper 100–200 m (e.g., no attempt was made to simulate the mixed layer stratification), based on mooring data that extended into the upper ocean, the procedure accurately replicated the depth of the upper bounding surface of Upper Labrador Sea Water ($\gamma_n = 27.8$ kg/m^3) using observed data from as deep as 1000 m.

Several extended gaps in the moored records are evident in Figure A1 during which no information was available: the longest being W2 from late 2008 to spring 2009, W4 from fall 2011 to fall 2012 and W6 before spring 2008 and in mid-2010. In the first two cases, daily profiles were synthesized by simple horizontal interpolation between the profiles from the two adjacent moorings. The present analysis considers no data from W6 prior to spring 2008 and no attempt was made to interpolate through the 2010 gap. Smaller gaps (e.g., between mooring settings) were filled by linear temporal interpolation.

Acknowledgments
The Line W research program was initiated by a grant from the G. Unger Vetlesen Foundation and support from the Woods Hole Oceanographic Institution. The main Line W observing program between 2004 and 2014 was funded by the US National Science Foundation with supplemental contributions from WHOI's Ocean and Climate Change Institute. We are grateful for this support and as well, acknowledge the efforts of a vast number of individuals who contributed to the collection, processing, and analysis of the Line W observations. Ruth Curry is deserving of particular thanks. This manuscript benefited from feedback from David Smeed and an anonymous reviewer. The individual sensor data from the Line W mooring program and the shipboard hydrographic data are available from the National Centers for Environmental Information (https://www.nodc.noaa.gov/) and OceanSITES (http://www.oceansites.org/data/). All data are also accessible from the Line W project website: http://www.whoi.edu/science/PO/linew/.

References

Andres, M. (2016), On the recent destabilization of the Gulf Stream Path downstream of Cape Hatteras, *Geophys. Res. Lett.*, *43*, 9836–9842, doi:10.1002/2016GL069966.

Andres, M., J. M. Toole, D. Torres, W. M. Smethie Jr., T. M. Joyce, and R. G. Curry (2016), Stirring by deep cyclones and the evolution of Denmark Strait Overflow Water observed at Line W, *Deep Sea Res., Part I*, *109*, 10–26, doi:10.1016/j.dsr.2015.12.011.

Andres, M., J. M. Toole, D. Torres, W. M. Smethie Jr., T. M. Joyce, and R. G. Curry (2017), Corrigendum to "Stirring by deep cyclones and the evolution of Denmark Strait Overflow Water observed at Line W" [Deep Sea Res. I 109, 10–26], *Deep Sea Res., Part I*, *121*, 245–248, doi:10.1016/j.dsr.2017.01.005.

Brown, O. B., P. C. Cornillon, S. R. Emmerson, and H. Mark Carle (1986), Gulf Stream warm rings: A statistical study of their behavior, *Deep Sea Res., Part A*, *33*, 1459–1473.

Bryden, H. L., W. E. Johns, and P. M. Saunders (2005), Deep Western Boundary Current east of Abaco: Mean structure and transport, *J. Mar. Res.*, *63*, 35–57.

Bryden, H. L., B. A. King, G. D. McCarthy, and E. L. McDonagh (2014), Impact of a 30% reduction in Atlantic Meridional overturning during 2009–2010, *Ocean Sci.*, *10*, 683–691, doi:10.5194/os-10-683-2014.

Clarke, R. A., R. M. Hendry, and I. Yashayev (1998), A western boundary current meter array in the North Atlantic near 42°N, *WOCE Newsl.*, *33*, 33–34.

Cunningham, S. A., et al. (2007), Temporal variability of the Atlantic meridional overturning circulation at 26.5°N, *Science*, *317*, 935–938, doi:10.1126/science.1141304.

Davis, X. J., T. M. Joyce, and Y.-O. Kwon (2017), Prediction of silver hake distribution on the Northeast U.S. shelf based on the Gulf Stream path index, *Cont. Shelf Res.*, *138*, 51–64.

Evans, D. G., J. Toole, G. Forget, J. D. Zika, A. C. Naveira Garabato, A. J. George Nurser, and L. Yu (2017), Recent wind-driven changes in the Atlantic meridional overturning circulation, *J. Phys. Oceanogr.*, *47*, 633–647, doi:10.1175/JPO-D-16-0089.1.

Flagg, C. N., M. Dunn, D.-P. Wang, H. T. Rossby, and R. L. Benway (2006), A study of the currents of the outer shelf and upper slope from a decade of shipboard ADCP observations in the Middle Atlantic Bight, *J. Geophys. Res.*, *111*, C06003, doi:10.1029/2005JC003116.

Forget, G., J.-M. Campin, P. Heimbach, C. N. Hill, R. M. Ponte, and C. Wunsch (2015), ECCO version 4: An integrated framework for non-linear inverse modeling and global ocean state estimation, *Geosci. Model Dev.*, *8*, 3071–3104, doi:10.5194/gmd-8-3071-2015.

Forget, G., J.-M. Campin, P. Heimbach, C. N. Hill, R. M. Ponte, and C. Wunsch (2016), *ECCO Version 4: Second Release*, MIT Libraries, Cambridge, Mass. [Available at http://hdl.handle.net/1721.1/102062.]

Fratantoni, P. S., and R. S. Pickart (2003), Variability of the shelf break jet in the Middle Atlantic Bight: Internally or externally forced?, *J. Geophys. Res.*, *108*(C5), 3166, doi:10.1029/2002JC001326.

Fuglister, F. C., and A. D. Voorhis (1965), A new method of tracking the Gulf Stream, *Limnol. Oceanogr.*, *10*, R115–R124, doi:10.4319/lo.1965.10.suppl2.r115.

Hansen, B., K. M. H. Larsen, H. Hátún, and S. Østerhus (2016), A stable Faroe Bank Channel overflow 1995–2015, *Ocean Sci.*, *12*, 1205–1220, doi:10.5194/os-12-1205-2016.

Jackett, D. R., and T. J. McDougall (1997), A neutral density variable for the world's oceans, *J. Phys. Oceanogr.*, *27*, 237–263.

Jackson, L. C., K. A. Peterson, C. D. Roberts, and R. A. Wood (2016), Recent slowing of Atlantic overturning circulation as a recovery from earlier strengthening, *Nat. Geosci.*, *9*, 518–522, doi:10.1038/ngeo2715.

Jochumsen, K., D. Quadfasel, H. Valdimarsson, and S. Jónsson (2012), Variability of the Denmark Strait overflow: Moored time series from 1996–2011, *J. Geophys. Res.*, *117*, C12003, doi:10.1029/2012JC008244.

Joyce, T. M. (1984), Velocity and hydrographic structure of a Gulf Stream warm-core ring, *J. Phys. Oceanogr.*, *14*(5), 936−947.

Joyce, T. M., and M. A. Kennelly (1985), Upper ocean velocity structure of Gulf Stream Warm Core Ring 82B, *J. Geophys. Res.*, *90*(C5), 8839−8844.

Joyce, T. M., C. Deser, and M. A. Spall (2000), The relation between decadal variability of subtropical mode water and the North Atlantic Oscillation, *J. Clim.*, *13*, 2250–2569.
Joyce, T. M., J. Dunworth-Baker, R. S. Pickart, D. Torres, and S. Waterman (2005), On the Deep Western Boundary Current south of Cape Cod, *Deep Sea Res., Part II*, *52*, 615–625.
Joyce, T. M., J. M. Toole, P. Klein, and L. N. Thomas (2013), A near-inertial mode observed within a Gulf Stream warm-core ring, *J. Geophys. Res. Oceans*, *118*, 1797–1806, doi:10.1002/jgrc.20141.
Kanzow, T., U. Send, W. Zenk, A. D. Chave, and M. Rhein (2006), Monitoring the integrated deep meridional flow in the tropical North Atlantic: Long-term performance of a geostrophic array, *Deep Sea Res., Part I*, *53*, 528–546, doi:10.1016/j.dsr.2005.12.007.
Koehl, A. (2015), Evaluation of the GECCO2 ocean synthesis: Transports of volume, heat and freshwater in the Atlantic, *Q. J. R. Meteorol. Soc.*, *141*, 166–181, doi:10.1002/qj.2347.
Le Bras, I. A. (2017), Dynamics of North Atlantic Western Boundary Currents, PhD dissertation, MIT/WHOI Joint Program, 174 pp., Woods Hole Oceanographic Institution, Woods Hole, Mass.
Le Bras, I. A., I. Yashayaev, and J. M. Toole (2017), Tracking Labrador Sea Water property signals along the Deep Western Boundary Current, *J. Geophys. Res. Oceans*, *122*, 5348–5366, doi:10.1002/2017JC012921.
Lee, T. N., W. Johns, F. Schott, and R. Zantopp (1990), Western boundary current structure and variability east of Abaco, Bahamas, at 26.5°N, *J. Phys. Oceanogr.*, *20*, 446–466.
Lee, T. N., W. E. Johns, R. J. Zantopp, and E. R. Fillenbaum (1996), Moored observations of western boundary current variability and thermohaline circulation at 26.5°N in the subtropical North Atlantic, *J. Phys. Oceanogr.*, *26*, 962–983.
McCarthy, G., E. Frajka-Williams, W. E. Johns, M. O. Baringer, C. S. Meinen, H. L. Bryden, D. Rayner, A. Duchez, C. Roberts, and S. A. Cunningham (2012), Observed interannual variability of the Atlantic meridional overturning circulation at 26.5°N, *Geophys. Res. Lett.*, *39*, L19609, doi:10.1029/2012/GL052933.
McCarthy, G. D., D. A. Smeed, W. E. Johns, E. Frajka-Williams, B. I. Moat, D. Rayner, M. O. Baringer, C. S. Meinen, J. Collins, and H. L. Bryden (2015), Measuring the Atlantic meridional overturning circulation at 26°N, *Prog. Oceanogr.*, *130*, 91–111, doi:10.1016/j.pocean.2014.10.006.
Mertens, C., M. Rhein, M. Walter, C. W. Böning, E. Behrens, D. Kieke, R. Steinfeldt, and U. Stöber (2014), Circulation and transports in the Newfoundland Basin, western subpolar North Atlantic, *J. Geophys. Res. Oceans*, *119*, 7772–7793, doi:10.1002/2014JC010019.
Peña-Molino, B., T. M. Joyce, and J. M. Toole (2011), Recent changes in the Labrador Sea Water within the Deep Western Boundary Current southeast of Cape Cod, *Deep Sea Res., Part I*, *58*, 1019–1030.
Peña-Molino, B., T. M. Joyce, and J. M. Toole (2012), Variability in the Deep Western Boundary Current: Local versus remote forcing, *J. Geophys. Res.*, *117*, C12022, doi:10.1029/2012JC008369.
Pérez-Hernández, M. D., and T. M. Joyce (2014), Two modes of Gulf Stream variability revealed in the last two decades of satellite data, *J. Phys. Oceanogr.*, *44*, 149–163, doi:10.1175/JPO-D-13-0136.1.
Rhein, M., D. Kieke, and R. Steinfeldt (2015), Advection of North Atlantic deep water from the Labrador Sea to the southern hemisphere, *J. Geophys. Res. Oceans*, *120*, 2471–2487, doi:10.1002/2014JC010605.
Savidge, D. K., and J. M. Bane Jr. (1999a), Cyclogenisis in the deep ocean beneath the Gulf Stream: 1. Description, *J. Geophys. Res.*, *104*(C8), 18,111–18,126.
Savidge, D. K., and J. M. Bane Jr. (1999b), Cyclogenisis in the deep ocean beneath the Gulf Stream: 2. Dynamics, *J. Geophys. Res.*, *104*(C8), 18,127–18,140.
Schott, F. A., and P. Brandt (2007), Circulation and deep water export of the subpolar North Atlantic during the 1990's, in *Ocean Circulation: Mechanisms and Impacts—Past and Future Changes of Meridional Overturning*, edited by A. Schmittner, J. C. H. Chiang, and S. R. Hemming, pp. 91–118, AGU, Washington, D. C., doi:10.1029/173GM08.
Schott, F. A., R. Zantopp, L. Stramma, M. Dengler, J. Fischer, and M. Wibaux (2004), Circulation and deep-water export at the western exit of the subpolar North Atlantic, *J. Phys. Oceanogr.*, *34*, 817–843.
Schott, F. A., J. Fischer, M. Dengler, and R. Zantopp (2006), Variability of the Deep Western Boundary Current east of the Grand Banks, *Geophys. Res. Lett.*, *33*, L21S07, doi:10.1029/2006GL026563.
Send, U., M. Lankhorst, and T. Kanzow (2011), Observation of decadal change in the Atlantic meridional overturning circulation using 10 years of continuous transport data, *Geophys. Res. Lett.*, *38*, L24606, doi:10.1029/2011GL049801.
Silverthorne, K. E., and J. M. Toole (2008), Seasonal kinetic energy variability of near-inertial motions, *J. Phys. Oceanogr.*, *39*, 1035–1049, doi:10.1175/2008JPO3920.1.
Smeed, D. A., et al. (2014), Observed decline of the Atlantic meridional overturning circulation 2004–2012, *Ocean Sci.*, *10*, 29–38, doi:10.5194/osd-10-29-2014.
Smith, J. N., W. M. Smethie Jr., I. Yashayev, R. Curry, and K. Azetsu-Scott (2016), Time series measurements of transient tracers and tracer-derived transport in the Deep Western Boundary Current between the Labrador Sea and the subtropical Atlantic Ocean at Line W, *J. Geophys. Res. Oceans*, *121*, 8115–8138, doi:10.1002/2016JC011759.
Srokosz, M. A., and H. L. Bryden (2015), Observing the Atlantic meridional overturning circulation yields a decade of inevitable surprises, *Science*, *348*, 1255575, doi:10.1126/science.1255575.
Stommel, H. M. (1957), A survey of ocean current theory, *Deep Sea Res.*, *4*, 148–184.
Thompson, R. (1971), Topographic Rossby Waves at a site north of the Gulf Stream, *Deep Sea Res. Oceanogr. Abstr.*, *18*, 1–19.
Toole, J. M., R. G. Curry, T. M. Joyce, M. McCartney, and B. Peña-Molino (2011), Transport of the North Atlantic Deep Western Boundary Current about 39°N, 70°W: 2004–2008, *Deep Sea Res., Part II*, *58*, 1768–1780.
Watts, D. R. (1991), Equatorward currents in temperatures 1.8–6.0°C on the continental slope in the Mid-Atlantic Bight, in *Deep Convection and Deep Water Formation in the Ocean*, edited by P. C. Chu and J. C. Gascard, pp.183–196, Elsevier Science, Amsterdam; New York.
Willis, J. K. (2010), Can in situ floats and satellite altimeters detect long-term changes in Atlantic Ocean overturning?, *Geophys. Res. Lett.*, *37*, L06602, doi:10.1029/2010GL042372.
Yang, J. (2015), Local and remote wind stress forcing of the seasonal variability of the Atlantic meridional overturning circulation (AMOC) transport at 26.5°N, *J. Geophys. Res. Oceans*, *120*, 2488–2503, doi:10.1002/2014JC010317.
Yashayaev, I., and J. W. Loder (2016), Recurrent replenishment of Labrador Sea Water and associated decadal-scale variability, *J. Geophys. Res. Oceans*, *121*, 8095–8114, doi:10.1002/2016JC012046.
Zantopp, R., J. Fischer, M. Visbeck, and J. Karstensen (2017), From interannual to decadal—17 years of boundary current transports at the exit of the Labrador Sea, *J. Geophys. Res. Oceans*, *122*, 1724–1748, doi:10.1002/2016JC012271.
Zou, S., and M. S. Lozier (2016), Breaking the linkage between Labrador Sea Water production and its advective export to the subtropical gyre, *J. Phys. Oceanogr.*, *46*, 2169–2182, doi:10.1175/JPO-D-15-0210.1.